The Linear Induction Motor(LIM) Power Factor, Efficiency and Finite Element Considerations.

E.B. dos Santos(Dr)[1], J.R. Camacho(PhD)[2], A.A. de Paula(MSc)[2] and C.H. Salerno(Dr)[2]

[1] Universidade Federal de Goias, School of Electrical Engineering,
74605-020 - Goiania - GO - Brazil,
email: ebs@eee.ufg.br

[2] Universidade Federal de Uberlandia, School of Electrical Engineering,
PO Box: 593, 38400-902 - Uberlandia - MG - Brazil,
email: jrcamacho@ufu.br

Abstract – **The aim of this work is to present a mathematical model for the linear induction motor, this model will allow us to estimate its efficiency, considering the winding space harmonics. This work followed the strategy of a research among rotary machines to find the one which could be the base of all the studies, the machine found was the rotary three-phase asymmetrical induction motor. This is justified by the inherent asymmetry characteristic of LIM that comes from building aspects. Experimental procedures with a LIM prototype makes viable the theoretical against experimental tests to make the validation for the proposed model. A special section will be dedicated of electromagnetic aspects of the LIM through finite element analysis.**

Keywords - linear, induction motor, finite elements.

1. Introduction

The main task in the course of this work was the development of a mathematical model which allows to obtain the efficiency of the LIM, in the case of the machine being fed by a constant voltage source.

The strategy in this case was to find a machine as a benchmark which could incorporate the natural asymmetry for the LIM. A long search ended up in the rotary asymmetrical three-phase induction motor, this is defensible by the natural asymmetry of the LIM that comes from building constraints. Internal electromagnetic aspects of the machine will be shown in a special section through the use of finite element analysis. The asymmetrical induction motor used in this work is an ordinary rotary machine with a squirrel-cage rotor and the stator having a different turns number in each of the phases. However, the LIM is a machine with straight and short primary and the winding being distributed in a single layer and concentric. The secondary (linor) for this motor is made of a circular aluminum plate. Therefore, taking in consideration the characteristics shown above a mathematical model is developed based in equivalence principles between the two mentioned machines. In this sense, when the machines are fed by the same line voltages, identical currents, force and speed should be observed in both machines.

2. Mathematical Model

In the mathematical model development are observed the equivalence principles already mentioned previously. Initially, attention is focused in the asymmetrical induction motor, where the turns number in each stator phase a, b, c are respectively N_a, N_b e N_c, and taking phase a as a reference, the following relations can be written:

$$b_1 = \frac{N_a}{N_b} \tag{1}$$

$$c_1 = \frac{N_a}{N_c} \tag{2}$$

Therefore, the unbalance factors b_1 and c_1, should assume values taking into consideration that the equivalence principles between the asymmetrical rotary induction motor and the linear induction motor should be satisfied.

The observation of the LIM, led us to the consideration of voltage and current time harmonics up to the 50^{th}, and the verification of total harmonic distortion lower than 0.2% allowed in this study the consideration of fundamental components only.

Through the use of a data acquisition system and Fast Fourier Transform (FFT), the following parameters were obtained:

- phase voltages $\dot{V}_a$, $\dot{V}_b$, $\dot{V}_c$, applied respectively to primary winding phases "a", "b" and "c";
- feeding line currents $\dot{I}_a$, $\dot{I}_b$, and $\dot{I}_c$ respectively for primary winding phases "a", "b" and "c".

Impedances respectively $\dot{Z}_a$, $\dot{Z}_b$, and $\dot{Z}_c$ for primary winding phases "a", "b" and "c" are obtained experimentally according procedures described in reference [2].

Therefore, the phase electromotive forces, $\dot{E}_a$, $\dot{E}_b$, and $\dot{E}_c$, respectively for phases "a", "b" e "c" are estimated from the following expression:

$$\begin{bmatrix} \dot{E}_a \\ \dot{E}_b \\ \dot{E}_c \end{bmatrix} = \begin{bmatrix} \dot{V}_a \\ \dot{V}_b \\ \dot{V}_c \end{bmatrix} - \begin{bmatrix} \dot{Z}_a & 0 & 0 \\ 0 & \dot{Z}_b & 0 \\ 0 & 0 & \dot{Z}_c \end{bmatrix} \begin{bmatrix} \dot{I}_a \\ \dot{I}_b \\ \dot{I}_c \end{bmatrix} \tag{3}$$

With the knowledge of electromotive induced forces, and with the use of symmetrical components for phase "a" as a reference a applying Faraday's Law, the following expression can be obtained:

$$\dot{E}_a + b_1\dot{E}_b + c_1\dot{E}_c = 0 \tag{4}$$

Values for b_1 and c_1 are real numbers, and the result of a unique solution for the two equation and two unknown

system composed the expressions originated from real and imaginary parts of equation 4. Through the knowledge of characteristic factors b_1 and c_1, taking as a basis the symmetrical components theory, and keeping phase "a" as an electrical reference, the following expression can be obtained:

$$\begin{bmatrix} \dot{E}_{ao} \\ \dot{E}_{ap} \\ \dot{E}_{an} \end{bmatrix} = \begin{bmatrix} 1 & 1 & 1 \\ 1 & a & a^2 \\ 1 & a^2 & a \end{bmatrix} \begin{bmatrix} \dot{E}_a \\ b_1\dot{E}_b \\ c_1\dot{E}_c \end{bmatrix} \quad (5)$$

where:

$$a = e^{j(2\pi/3)} \quad (6)$$

and being $\dot{E}_{a0}$ identically zero.

With the knowledge of vectors $\dot{E}_{ap}$, $\dot{E}_{an}$ and the power transferred to the linor (secondary), the corresponding positive and negative sequence feeding current components ($\dot{I}_{ap}$ and $\dot{I}_{an}$). Taking into consideration also the winding space harmonics, the magnetization reactances are also obtained, the *h* index is the space order harmonics. The linor impedances referred to the primary are obtained based on equations (7) and (8).

$$\dot{Z'}^{+}_{2h} = R'_{2h} + js^{+}_{h}.X'_{d2h} \quad (7)$$

$$\dot{Z'}^{-}_{2h} = R'_{2h} + js^{-}_{h}.X'_{d2h} \quad (8)$$

where:

$$\mathrm{s}^{+}_{\mathrm{h}} = 1 - \mathrm{h}(1 - \mathrm{s}) \quad (9)$$

$$\mathrm{s}^{-}_{\mathrm{h}} = 1 + \mathrm{h}(1 - \mathrm{s}) \quad (10)$$

The above reactances and impedances are obtained experimentally according to the no-load and locked linor tests as described in reference [6]. Propelling forces are determined through the superposition of space harmonic effects in the windings. Therefore, the active power through the air-gap (P_{ph} and P_{nh}) due the h_{th} harmonic magnetomotive force (*mmf*) space distribution are given by:

$$P_{ph} = 3.I^2_{ap}.\Re e\left(\dot{Z}_{aph}\right) \quad (11)$$

$$P_{nh} = 3.I^2_{an}.\Re e\left(\dot{Z}_{anh}\right) \quad (12)$$

for $h = 6n+1$ with $n = 0, 1, 2, 3, 4...$ in equations (11) and (12), and also:

$$P_{ph} = 3.I^2_{ap}.\Re e\left(\dot{Z}_{anh}\right) \quad (13)$$

$$P_{nh} = 3.I^2_{an}.\Re e\left(\dot{Z}_{aph}\right) \quad (14)$$

for $h = 6n + 1$ with $n = 0, 1, 2, 3, 4...$ in equations (13) and (14). The linear synchronous speed (v_{sh}), relative to the h_{th} harmonic order, is obtained through the following equation:

$$v_{sh} = \frac{v_s}{h} \quad (15)$$

v_s is the linear synchronous speed, relative to the fundamental space harmonic, which is obtained through a product of the polar step times the frequency in the mains. Therefore, the propelling forces from the positive (F_{uph}) and negative (F_{unh}) sequence systems, according equations (16) and (17) as follows:

$$F_{uph} = \frac{P_{ph}}{v_{sh}} \quad (16)$$

$$F_{unh} = -\frac{P_{nh}}{v_{sh}} \quad (17)$$

A resulting propelling force is given by:

$$F = \sum_h (F_{uph} + F_{unh}) \quad (18)$$

Application of the proposed model consists on the initial calculation of asymmetrical and symmetrical components of positive and negative sequence currents, from applied terminal voltages. So, the equations used are the ones which relates phase voltages and the mentioned current components. With the knowledge of primary windings and linor phase impedances, also knowing the characteristic factors b1 and c1 and the unbalancing factor which relates the positive and negative sequence components for the current of the reference phase. Impedances and factors are determined experimentally. So, it will be possible to obtain the feeding current and propelling force. The efficiency and power factor are obtained as follows.

Through the use of $\dot{V}$ and $\dot{I}$ to denote the line voltage and line current vectors respectively, we have:

$$I = \begin{bmatrix} \dot{I}_a \\ \dot{I}_b \\ \dot{I}_c \end{bmatrix} \quad (19)$$

$$V = \begin{bmatrix} \dot{V}_a \\ \dot{V}_b \\ \dot{V}_c \end{bmatrix} \quad (20)$$

With I^* being the complex vector $\dot{I}$ with opposed signal imaginary part, and V^t the transpose of vector $\dot{V}$, the complex power delivered to the machine will be designated by which is given by:

$$\dot{S} = V^t.I^* \quad (21)$$

From equation (6) can be extracted the active power (P) as in equation (22).

$$P = \Re e(\dot{S}) \quad (22)$$

With the knowledge of total and active powers can be obtained the power factor (*pf*) according to equation (23).

$$pf = \frac{P}{S} \quad (23)$$

where S is the absolute value of $\dot{S}$. From the speed of moving part (v_x), which in this case is the linor, and the corresponding propelling force (F), the power output is obtained through the following equation:

$$P_o = F.v_x \tag{24}$$

The values of P and P_o make it possible to estimate the efficiency (η) through the following expression:

$$\eta = \frac{P_o}{P} \tag{25}$$

3. The Prototype

The LIM prototype used in this work is a three phase, two pole, tow packages and short primary. The primary packages (stator) are made of oriented steel sheets, and the linor(stator) is made of a non-magnetic material (aluminum) in a flat disk shape.

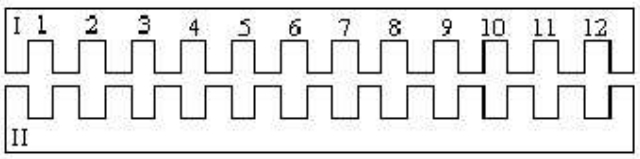

Fig. 1. Double core view for the LIM primary, packages I and II without winding.

The primary packages are made of open type slots, with all being equally filled. However, every package has twelve slots, being two per pole per phase. To illustrate such situation, Figure (1) shows the format and slot distribution in the primary packages.

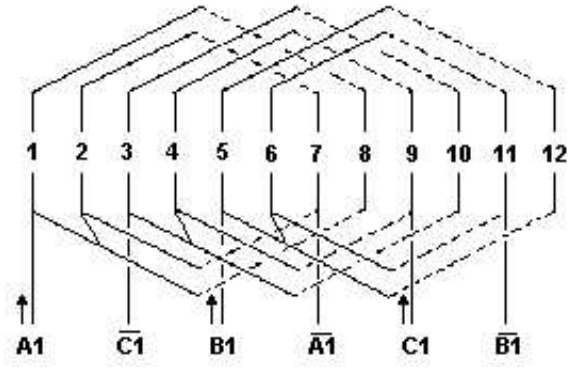

Fig. 2. Double core view for the LIM primary, packages I and II without winding.

The winding in each primary package has the following configuration: three-phase, single layer, concentric, with coils in groups of two. Each coil has one hundred turns of cooper conductors with transversal section area of $0,519mm^2$, with steps 1:8 and 2:7. The winding scheme can be seen in Figure (2).

Winding terminals for package II are: $A2$, $\bar{C}\bar{2}$, $B2$, $\bar{A}\bar{2}$, $C2$ and $\bar{B}\bar{2}$.

4. Theoretical and Experimental Validation

From the machine electrical terminals parameters were obtained (voltage and current signals) with a data acquisition system. To measure the speed a micro-controlled encoder with an optical active sensor was used. To obtain the applied forces was used a dc generator, and the efficiency was obtained through the feeding of a resistive load bank. The computed values were obtained with the developed model. Table 1 shows the values of the impedances for the primary winding phases, obtained experimentally.

Table I - Primary Impedances.

Phase	Impedance (Ω)
a	5,348 + j5,729
b	5,354 + j5,903
c	5,128 + j6,052

Table II shows values obtained experimentally for the magnetization reactance and secondary impedance referred to the primary, both for phase "*a*", the reference phase. It is convenient to highlight that the mentioned values are referred only to the fundamental space component, with the machine at the conditions of no-load and locked linor.

Table II - Values of X_{gl}, Z_{21}^{+} and Z_{21}^{-}.

X_{gl} (Ω)	Z_{21}^{+} (Ω)	Z_{21}^{-} (Ω)
35,0434	11,3586+j1,2954	11,3586+j1,2954

Graphs of Figures (3) and (4) depict the behavior of measured and calculated values of efficiency (Effic.) and power factor (PF), both as a function of $(1-s)$ where s is the slip.

For the theoretical and experimental validation a three-phase, flat, two-poles, a two-side short-primary LIM was used. The oriented steel-silicon primary packages (stator) and the secondary (linor) constituted of a non-magnetic material, the aluminum, in a disk shape.

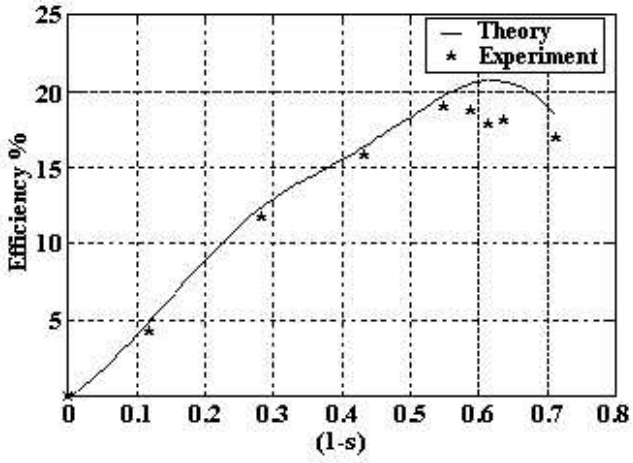

Fig. 3. Efficiency against $(1-s)$.

The experimental data was obtained from a data acquisition system. For the speed measurement an active optical micro-processed encoder was used. To obtain the applied forces a dc generator feeding a bulk of resistive loads, where the efficiency has been measured. The calculated values were obtained through the use of the developed model.

5. Finite Elements Considerations

In order to obtain the unbalanced parameters for the linear induction used in experimental tests, the machine was accurately characterized in two two dimension figures: one in the

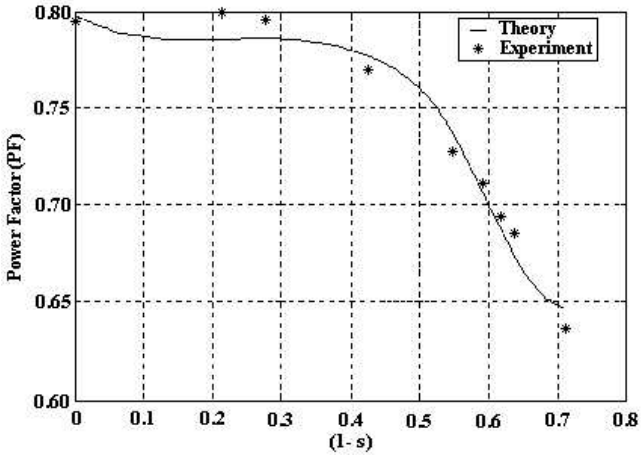

Fig. 4. Power factor against $(1 - s)$.

xy plane, a view from above, and the other in the *yz* transverse plane. The transverse view turned to be necessary, since in the linear motor, the coil heads are of reasonable dimension when compared with the coil region immersed in the magnetic material. Therefore they have a substantial contribution to the stator leakage reactance. The current density in each slot is of $2.5A/mm^2$ and the current considered nominal is $2A$. The magnetic core is made of 0.27mm tick M4 silicon-steel sheets and the the magnetic characteristic can be seen in figure 5. When obtained machine parameters through the use of finite elements the machine will be considered in two main situations:

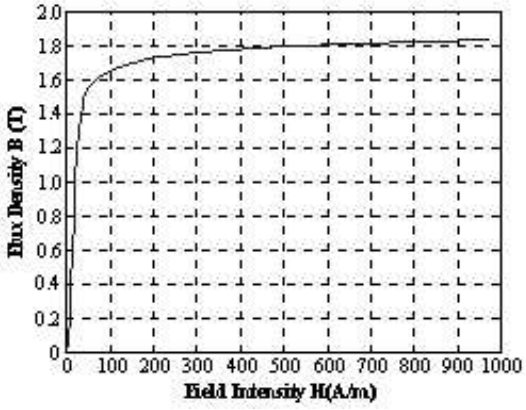

Fig. 5. Saturation characteristic for the M4 oriented silicon-steel core.

- the static magnetic problem, in which the fields are not variant in time ($f = 0Hz$). In this condition, the magnetic field (H) and the magnetic flux density (B) must comply with:

$$\nabla \times H = J \tag{26}$$

$$\nabla . B = 0 \tag{27}$$

where J is the current density, constrained to the following elementary relationship:

$$B = \mu H \tag{28}$$

With the flux density expressed in terms of vector magnetic potential A:

$$B = \nabla . A \tag{29}$$

Equation (26) can be written as:

$$\nabla \times (1/\mu . \nabla \times A) = J \tag{30}$$

since the materials used are linear and isotropic the equation can be reduced to:

$$-1/\mu . \nabla^2 . A = J \tag{31}$$

In this case the analysis is $2D$ and the vector A has only one component ortogonal to the plane in question. With the knowledge of vector A, B and H can be obtained trough the differentiation of A. In order to represent the machine at no-load condition the rotor (linor) is pulled out. Being a static magnetic case only the real part of current density is used.

The magnetization reactance in each phase can be obtained through the computation of the stored energy in each coil:

$$x_m = \omega . N^2 . 2 . E_m . h / i^2 \tag{32}$$

where x_m is the magnetization reactance for each phase, ω is the angular frequency in rd/s, N is the per pole per phase turns number, h is the magnetic core length and E_m is the stored magnetic energy in the mentioned coil in J/m.

- the harmonic problem ($f = 60Hz$), in this case the fields are changing in time, and induced currents can be seen in the materials with non-zero conductivity. Through the representation of electric field by E and the current density by J, E and J must comply with the following relationship:

$$J = \sigma E \tag{33}$$

Therefore, the induced electric field is given by:

$$\nabla \times E = -\partial B / \partial t \tag{34}$$

this can also be written as:

$$\nabla \times E = -\nabla \times A \tag{35}$$

In the case of the $2D$ problem, the equation (35)can be integrated anterior pode ser integrada to satisfy equation (36).

$$E = -A - \nabla V \tag{36}$$

that taken into equation (33) results:

$$J = -\sigma A - \sigma \nabla V \tag{37}$$

and substituted in (31) give us the following partial differential equation:

$$1/\mu.\nabla^2.A = \sigma A - J_{exc} + \sigma \nabla V \tag{38}$$

where J_{exc} being the representation of the excitation current source applied and ∇V is the an additional potential gradient, in $2D$ problems it is constant over a conducting body.

In the parameter determination with blocked linor, equation (38) is used for the computation of the vector magnetic potential A.

The coil resistances can be obtained doing the computation of the energy dissipated in the coils by the Joule effect (P_j) through the finite elements program using equation (39):

$$r = P_j.h/i^2 \tag{39}$$

The leakage reactance in each phase is obtained by inputting current in only one coil of each package phase. It is mandatory in the calculation that we must not have coupling with the other phases, with this purpose the cooper conductivity is made zero. In order to use in the leakage reactance calculation the same current as in the laboratory test, the conductor conductivity in the coil is made equal to zero. The aluminum disk conductivity is also adjusted to an adequate value according to the disk temperature.

By plotting the magnetic flux lines distribution it is possible to obtain a k_d factor which represents the relationship between the flux lines that do not touch the linor (rotor) and the total number of flux lines. It is necessary, with this purpose, that a large number of lines should be plotted to obtain a k_d factor that is as accurate as possible. Figure (6), the machine view from above, and figure (7), the transverse view, shows the flux lines distribution for the phase *a* coil of one of the packages. Therefore, the stator leakage reactance in each package phase is given by:

$$x_d = k_d.\omega.h.(A_d - A_e)/i^2 \tag{40}$$

where A_d and A_e are the average value for the magnetic vector potential in the coil *right* and *left* leg respectively in each plane of analysis.

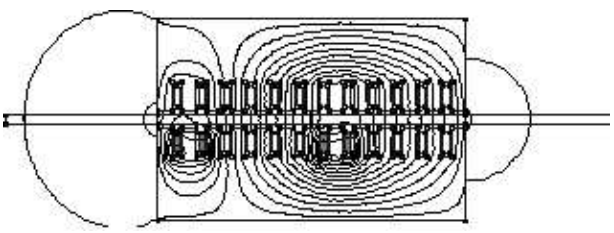

Fig. 6. Flux lines distribution for phase *a* in one of the packages, superior view.

To obtain the machine rotor (linor) parameters it is used the finite elements program by computing the resistive losses and magnetic energy in the rotor and shifting the result to the stator through the stator/linor transformation relationship. Figure (8) shows the linor induction when only the phase *a* is excited. To perform the calculation it is necessary to make sections in the linor in the regions where the currents have the same direction.

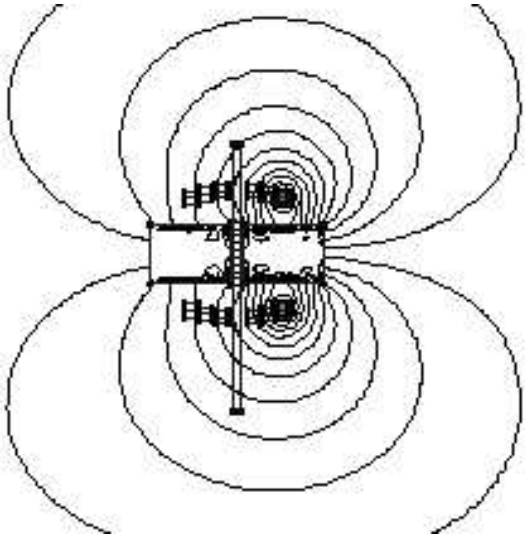

Fig. 7. Flux lines distribution for phase *a* in one of the packages, transverse view.

The table below shows the stator impedances, the linor impedance and magnetization reactance as seen from the stator obtained through the finite elements analysis for each phase.

Table III - Impedances and reactances obtained from FEM.

Phase	Z_s (Ω)	Z_r (Ω)	X_m (Ω)
a	5,3497+j5,5723	11.9218+j1,2192	35,2943
b	5,3312+j5,7579	8.1952+j1,7683	36,6294
c	5,3405+j5,7958	5,4853+j0.7345	18,5433

Z_s, Z_r and X_m in Table II are respectively the stator and rotor impedance, and the magnetization reactance for phases *a*, *b* and *c*. It can be clearly noted that the Linear Induction Motor has an unbalanced three-phase circuit and should be represented with a different single-phase circuit for each phase.

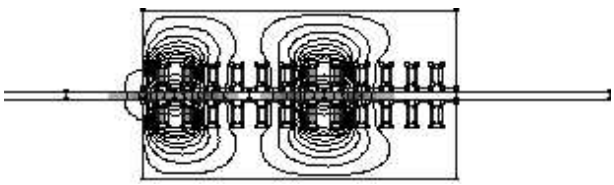

Fig. 8. Linor induction when only the phase *a* is excited.

Figure (9)shows the machine at no-load condition. The imposed currents to the machine in the simulation were: $I_a = 1,4902 \langle -56,62^o\ A$; $I_b = 1,5297 \langle 161,62^o\ A$; $Ic = 0,9897 \langle 50.32^o\ A$.

Figure (10) shows the machine at locked linor condition. The imposed currents to the machine in the simulation were:

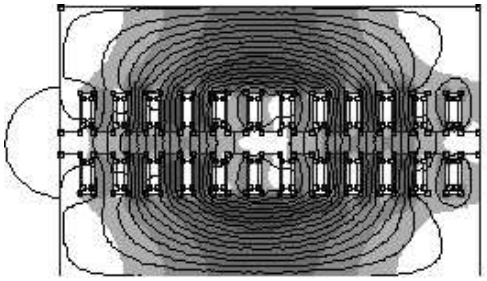

Fig. 9. Machine at no-load condition.

$Ia = 3,0914 \langle 113,33^o\ A$; $Ib = 3,0862 \langle -20.72^o\ A$; $Ic = 2,4110 \langle -133,58^o\ A$.

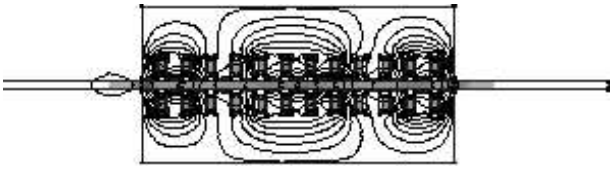

Fig. 10. Machine at locked linor condition.

With the blocked machine was computed the propelling force applied to the linor through the use of the Maxwell tensor analysis and the obtained result was equal to $F = 12.0881N$, very close to the value measured in the laboratory that was $F = 12.0562N$.

6. Conclusion

The model is then validated through de small differences between theoretical and experimental results, either in respect of electrical terminals through current values or the mechanical terminal through the value for the propelling forces. The static and dynamic end effects are modelled through the characteristic factors (b_1, c_1 and unbalance factor), making clear the dependence of the speed for these factors. The inclusion of winding space harmonics produced good results. Values for the efficiency can be observed in the graph of Figure (3), and also the power factor according to the graph in Figure (4). The results are justified by the relatively wide air-gap ($10.7mm$) and by the end effects due to the small pole numbers and the machine topology, objective of this work. However these characteristics allowed a thorough evaluation of the proposed model. Despite the fact that the line voltage system applied to the machine was rigorously balanced, an unbalance in the phase voltage system and also in the current system was observed at the machine's terminals. Both situations were due to the end effects from the design aspects for the machine under scrutiny.

References

[1] E.B. Santos,*Linear Induction Motor Analysis Based on the Equivalence With the Asymmetrical Rotary Induction Motor*, Universidade Federal de Uberlandia, Doctoral Thesis, Uberlandia, MG, Brazil, 2000.(In Portuguese)

[2] L.M. Neto, E.B. Santos, and J.R. Camacho, *Linear Induction Motor Parameter Determination on Force Development Application*, in *Proc. IEEE-Winter Meeting*, Singapore, 2000.

[3] E.B. Santos, L.M. Neto, and J.R. Camacho, *Linear Induction Motor Modeling and the Equivalence with the Asymmetrical Rotary Induction Motor*, in *Proc. ICEM2000-International Conference on Electrical Machines*, 2000, Espoo, Finland, pp. 242–246.

[4] G.F. Gieras, *Linear Induction Drivers*, Clarendon Press, Oxford (1994).

[5] S. Yamamura, et all., "Analysis of Linear Induction Motors with Discreet Winding and Finite Iron Length",*IEEE Trans. on PAS*, Vol. 91, pp. 1700–1710, 1972.

[6] J.K. Dukowicz, "Theories of the Linear Induction Motor and Compensated Linear Induction Motor",*IEEE Trans. on PAS*, Vol. 96, pp. 66–73, 1977.

[7] R.L. Russel and K.H. Norsworth, "Eddy Currents and Wall Losses in Screened-rotor Induction Motors", *Proc. of IEE*, pp. 163–175, 1958.

[8] H. Bolton, "Transverse Edge Effect in Sheet-rotor Induction Motors", *Proc. of IEE*, Vol. 116, n. 5, pp. 725–731, 1969.

[9] D. Meeker, *Finite Element Method Magnetics*, Version 3.1 User's Manual, September, 2001.

[10] T. Utsumi,I. Yamaguchi, T. Igari, and S. Shinoda,"Parameter-Value Evaluation of 3-phase Equivalent Circuit of Linear Induction Motor", *Proc. of the 1999 IEEE International Symposium on Diagnostics for Electrical Machines, Power Eletronics and Drives*, Gijon, Spain, pp. 275–280, September 1999.